

# 1 **Diel and seasonal methane dynamics in the shallow and** 2 **turbulent Wadden Sea**

3  
4 Tim R. de Groot <sup>1</sup>, Anne M. Mol <sup>1</sup>, Katherine Mesdag <sup>2</sup>, Pierre Ramond <sup>1,3</sup>, Rachel Ndhlovu <sup>1</sup>,  
5 Julia C. Engelmann <sup>1</sup>, Thomas Röckmann <sup>2</sup> and Helge Niemann <sup>1,4,5</sup>

6 1. Royal Netherlands Institute for Sea Research (NIOZ), Texel, the Netherlands

7 2. Institute for Marine and Atmospheric Research Utrecht (IMAU), Utrecht University, Utrecht, The Netherlands

8 3. Instituto de Ciencias del Mar (ICM), Barcelona, Spain

9 4. Department of Earth Sciences, Utrecht University, Utrecht, The Netherlands

10 5. Centre of Arctic Gas Hydrate, Environment and Climate (CAGE), UiT the Arctic University of Norway,  
11 Tromsø, Norway

12  
13 Correspondence to: Tim de Groot (tim.de.groot@nioz.nl)

14  
15 **Abstract.** The Wadden Sea is a coastal system fringing the land-sea borders of Denmark, Germany, and the  
16 Netherlands. The Wadden Sea is extremely productive and influenced by strong variations in physical and  
17 biological forcing factors that act on time scales of hours to seasons. Productive coastal seas are known to dominate  
18 the ocean's methane emission to the atmosphere, but knowledge on controls and temporal variations of methane  
19 dynamics in these vastly dynamic systems are scarce. Here we address this knowledge gap by measuring methane  
20 inventories and methanotrophic activity at a temporal resolution of two hours over a time period of two days,  
21 repeatedly during four successive seasons in the central Dutch Wadden Sea. We found that methane dynamics  
22 varied between colder and warmer seasons, with generally higher water column methane concentrations and  
23 methanotrophic activity in the warmer seasons. Efflux of methane to the atmosphere was, on the other hand, lower  
24 in the warmer seasons because of lower wind speeds. On a diel scale, tides controlled methanotrophic activity,  
25 which increased ~ 40 % at low tide compared to high tide. We estimate that methane oxidizing bacteria reduce the  
26 methane budget of the Dutch Wadden Sea by only 2 %, while ~ 1/3 escapes to the atmosphere and ~ 2/3 are flushed  
27 out into the open North Sea at ebb tide. Our findings indicate that tides play a key role in controlling methane  
28 dynamics and methanotrophic activity and highlight the importance of high resolution and repeated sampling  
29 strategies to resolve methane dynamics in fast-changing coastal systems.

## 30 1 Introduction

31

### 32 1.1 Methane and methane oxidation

33 Atmospheric methane (CH<sub>4</sub>) concentrations have been increasing since industrial times, surpassing 1900 ppb in  
34 2021 (Lan et al., 2022) and contributing more than 20 % of total radiative forcing in the atmosphere (Etminan et  
35 al., 2016). Due to its relative short atmospheric lifetime of ~10 years (Canadell et al., 2021), reducing methane  
36 emissions to the atmosphere could play a key role in global warming mitigation strategies. However,  
37 implementation of such strategies requires a thorough understanding of methane sources and sinks. Anthropogenic  
38 methane emissions (336 – 376 Tg y<sup>-1</sup>) are rather well constrained and constitute ~60 % of the total atmospheric  
39 budget (Saunois et al., 2020). Individual natural sources, on the other hand are associated with comparably large  
40 uncertainties. This is particularly true for methane emissions originating from marine environments (5 to 28 Tg  
41 CH<sub>4</sub> y<sup>-1</sup>; (Rosentreter et al., 2021)).

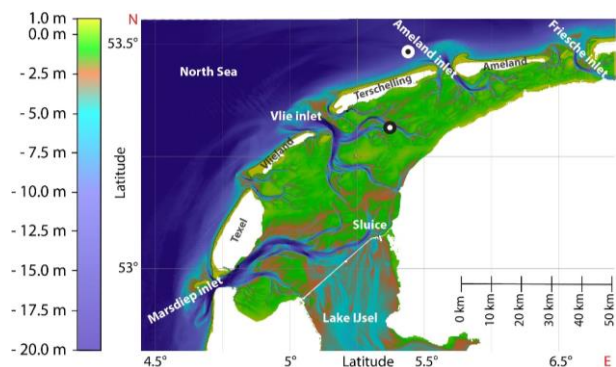
42 The inner shelf (0 – 50 m water depth) only account for ~ 3 % of the global ocean surface but are a main source  
43 of marine methane emissions to the atmosphere (Weber et al., 2019). In these shallow ecosystems, light availability  
44 as well as terrestrial inputs of nutrients support a high diversity of producers and consumers that generate huge  
45 quantities of organic matter (Philippart et al., 2009; Beck and Brumsack, 2012). Consequently, rates of organic  
46 matter degradation, including methanogenesis in anoxic sediments are high, often leading to elevated levels of free  
47 and dissolved methane in sediments and pore waters (Bange et al., 1994; Røy et al., 2008; Wu et al., 2015).  
48 Transport of methane-rich porewaters and ebullition of methane bubbles, in return, lead to elevated methane  
49 concentrations in the water column (Reeburgh, 2007; Grunwald et al., 2009; James et al., 2016). It is estimated  
50 that ~ 5 % of shelf seas surface waters have methane concentrations above 100 nM (Weber et al., 2019).  
51 Nevertheless, a substantial amount of dissolved methane is oxidized by aerobic methanotrophic bacteria (MOB),  
52 which mediate the aerobic oxidation of methane (MOx) (Reeburgh, 2007):



54 Similar to other metabolic processes involving small molecules, MOx discriminates against isotopically heavy  
55 methane (i.e. containing <sup>13</sup>C and <sup>2</sup>H (D) instead of <sup>12</sup>C and <sup>1</sup>H) so that the residual methane pool successively  
56 becomes <sup>13</sup>C and D enriched as a result of ongoing MOx (Barker and Fritz, 1981; Whiticar, 1999).

57 MOB typically belong to the Gamma- (type I and type X), Alphaproteobacteria (type II), Verrucomicrobia and  
58 members of candidate division NC10 (Hanson and Hanson, 1996; Knief, 2015). MOB build a microbial methane  
59 filter in the water column that functions as the ultimate sink for oceanic methane before reaching the atmosphere.  
60 Yet, little is known about the controls and capacity of this microbial filter in the inner shelf ecosystems where the  
61 vertical distance between the sedimentary source and the atmosphere is short. Factors such as oxygen (Boetius and  
62 Wenzhöfer, 2013; Steinle et al., 2017) and methane availability (Mau et al., 2013; James et al., 2016) affect MOx,  
63 but also increasing water temperatures play a role by impacting metabolic rates of MOB (He et al., 2012). The  
64 capacity of the microbial methane filter in the water column is typically higher during extended periods of  
65 continuity, i.e., when the water column is more stagnant (Steinle et al., 2015; James et al., 2016). This increases  
66 the contact time of MOB with methane-rich waters so that the size of the MOB standing stock increases. However,  
67 water mass movement induced by destratification, or seasonal winds, leads to shifting mixing regimes that disrupt  
68 continuity on a seasonal scale (Gründger et al., 2021). On a daily scale, tides induce currents, which also disrupt  
69 continuity and hence can affect MOx, too (Steinle et al., 2015). This disruption of continuity is particularly strong  
70 in the extremely dynamic inner-shelf seas where rapid changes in environmental conditions can lead to rapid  
71 changes in water column dynamics.

72 The Wadden Sea, a UNESCO heritage site that consists of the largest continuous tidal flat area worldwide (14.900  
73 km<sup>2</sup>), is an extremely dynamic system, with major hydrological changes occurring at seasonal to diel time scales.  
74 The Wadden Sea stretches for about 500 km along the coast of the Netherlands, Germany and Denmark. Here, we  
75 investigated methane dynamics in the Dutch part of the Wadden Sea, that is separated from the North Sea by five  
76 barrier islands (Fig. 1). Our aim was to temporally resolve methane dynamics from an hourly to a seasonal scale  
77 to determine key controls on methane dynamics and to establish a methane budget for the Dutch Waddensea



78

79 **Figure 1.** Bathymetry of the western sector of the Dutch Wadden Sea between the Marsdiep and Friesche inlet (modified from  
 80 Materić et al., 2022). Tidal inlets between barrier islands facilitate water exchange with the open North Sea. The time-series  
 81 station is located south of the island Terschelling (black mark; 53°19.015 N, 5°22.071 E). The offshore reference station is  
 82 located 8 km north of Terschelling (white mark; 53°29.190 N, 5°21.449 E).

## 83 2 Materials and methods

### 84 2.1 Experimental design

85 A chain of 5 barrier islands (located 5 to 30 km offshore) shelters the Dutch Wadden Sea from waves and strong  
 86 westerly winds. Between these barrier islands and with the rhythm of the tides, large volumes of water are  
 87 transported in and out the Dutch Wadden Sea through deep tidal inlets, such as the Marsdiep (most western point  
 88 of the Dutch Wadden Sea) and the Vlie inlet (Duran-Matute et al., 2014). Our fixed mooring station (53°19.015  
 89 N, 5°22.071 E) is in a branch of the Vlie inlet between the island of Terschelling and the mainland, roughly in the  
 90 middle of the Dutch Wadden Sea (Fig. 1). This location was chosen as it remains submerged at low tide and lays  
 91 in-between the Wadden Sea's landward and offshore termination. The water flowing by this station thus equally  
 92 integrates the tidal flat area, mostly during ebb tide, as well as the inflowing North Sea water during high tide.  
 93 Also, the station was relatively far away from the port of Harlingen (~ 20 km) so that a potential influence of  
 94 methane rich port waters is minimized. The reference station was located 8 km north of the island Terschelling in  
 95 the North Sea (53°29.190 N, 5°21.449 E).

96 Samples were recovered with the R/V Navicula during 4 sampling campaigns, respectively in winter (19 February  
 97 2019 – 21 February 2019), spring (23 April 2019 – 25 April 2019), summer (22 July 2019 – 24 July 2019) and  
 98 autumn (11 November 2019 – 13 November 2019). During each campaign, we conducted hourly CTD casts with  
 99 discrete water sampling over a two-day period. During CTD casts, water mass properties (temperature, salinity,  
 100 depth) and oxygen concentrations were measured continuously using a Sea-Bird (SBE911) + conductivity–  
 101 temperature–depth (CTD) system. Discrete water samples were recovered with Niskin bottles from 1 and 3 m  
 102 water depth and, upon recovery, immediately sampled for subsequent analyses of water column constituents  
 103 (methane concentrations, methane isotopic composition and methane oxidation rates).

104 Sediment samples were retrieved using a boxcorer, and upon recovery, subsampled with small pushcores (diameter  
 105 7 cm, ~ 18 cm sediment recovery). Pushcores were subsampled for methane concentrations by taking every 2 cm  
 106 5 mL of sediment that was quickly added to 60 mL glass bottles containing 30 mL of a saturated NaCl brine  
 107 solution and the bottles were immediately sealed with butyl rubber stoppers. Atmospheric flask samples (250 ml)  
 108 were taken hourly at ~ 10 m above the sea surface, in winter and spring. In summer and autumn, atmospheric  
 109 methane concentrations were continuously measured using a cavity ringdown spectrometer (CRDS, Picarro model  
 110 G2301).

### 111 2.2 Dissolved methane concentrations and stable isotope ratios

112 Dissolved methane concentrations were determined using a headspace (HS) technique (Green, 2005). In brief,  
 113 immediately upon CTD recovery, 260 mL glass serum bottles were filled HS-free, closed with black-butyl rubber  
 114 stoppers (Rubber B.V. the Netherlands) and crimp-top sealed. Next, we added a 5 mL N<sub>2</sub> headspace and fixed the  
 115 sample with 5 mL NaOH solution (25 % w/v). HS methane concentrations of sediments and dissolved methane  
 116 were measured in our home laboratories with a gas chromatograph (GC; Thermo Scientific FOCUS GC equipped  
 117 with a Restek stainless steel column HS-Q 80/100 SS GEN config (length 2 m, 2 mm ID, 1/8 OD) with flame  
 118 ionization detection). The instrument was calibrated with a certified 100 ppm methane standard (Scott Specialty  
 119 Gases Netherlands B.V.).

120 Similarly, seawater aliquots were taken for methane stable carbon and hydrogen isotope measurements, but these  
 121 samples were fixed with 60  $\mu\text{l}$   $\text{HgCl}_2$  (2 mM). A continuous flow isotope ratio mass spectrometry (CF-IRMS)  
 122 system was used to quantify D- $\text{CH}_4$  in the gas phase (Thermo Delta Plus XL, Thermo Fisher Scientific Inc.,  
 123 Germany) as described previously (Röckmann et al., 2016; Jacques et al., 2021). Isotopic values are represented  
 124 in the delta notation against the international reference standard VSMOW ( $\delta\text{D}$ ). To monitor precision and  
 125 accuracy, sample measurements were alternated with measurements of an inhouse air standard (cross calibrated  
 126 against certified reference standards) containing 1975.5 ppb methane with a  $\delta\text{D}$   $-90.81 \pm 1.1$  ‰. We constructed a  
 127 two-endmember mixing model (Mariotti et al., 1981; Jacques et al., 2021) and a Rayleigh fractionation model.  
 128 This was done to investigate whether enrichment of D in the residual methane was caused by MOx, which is  
 129 known to discriminate against heavy isotopes (Barker and Fritz, 1981; Whiticar, 1999), or by mixing with  
 130 comparably heavy atmospheric methane (see supplementary methods).

131

### 132 2.3 Methane oxidation rate measurements

133 MOx was determined by ex-situ incubations with trace amounts of  $^3\text{H}$ -labelled methane as described previously  
 134 (Niemann et al., 2015). Briefly, aliquots from each Niskin bottle were filled HS-free in 20 mL glass vials in  
 135 triplicate, sealed with grey-bromobutyl stoppers that are known to not hamper methanotrophic activity and  
 136 amended with 5  $\mu\text{L}$  of  $^3\text{H}\text{-CH}_4/\text{N}_2$  (4.5 kBq, American Radiolabeled Chemicals, USA). The samples were  
 137 incubated in a temperature-controlled incubator for 72 hours in the dark, maintaining in situ temperature  
 138 conditions. Activities of residual  $\text{C}^3\text{H}_4$  and the MOx product  $^3\text{H}_2\text{O}$  were measured by liquid scintillation counting.

139 MOx first-order rate constant ( $k$ ) was determined from the fractional tracer turnover (Reeburgh, 2007):

$$140 \quad k = \frac{{}^3\text{H}_2\text{O}}{{}^3\text{H}_2\text{O} + \text{C}^3\text{H}_4} \times \frac{1}{t} \quad (2)$$

141

142 where  $t$  is incubation time in days.  $k$  was corrected for (negligible) tracer turnover in killed controls (KC, fixed  
 143 with 100  $\mu\text{l}$   $\text{HgCl}_2$  directly after sampling) and multiplied with dissolved methane concentrations  $[\text{CH}_4]$ , yielding  
 144 MOx:

$$145 \quad \text{MOx} = (k - k_{\text{KC}}) \times [\text{CH}_4] \quad (3)$$

146

### 147 2.4 Diffusive fluxes of methane

148 The diffusive sea-air methane flux was calculated based on a boundary layer model that consider the relation  
 149 between wind, temperature and methane concentrations in the atmosphere and a well-mixed surface water layer  
 150 (Wanninkhof, 2014):

$$151 \quad F = (p\text{CH}_{4w} - p\text{CH}_{4a}) K_0 k_{\text{CH}_4} \quad (4)$$

152  $F$  denotes the diffusive methane flux,  $p\text{CH}_{4a}$  and  $p\text{CH}_{4w}$  (in atm) are the partial pressures of methane in the air and  
 153 in the well-mixed surface water layer, respectively.  $p\text{CH}_{4a}$  was measured with a Picarro G2301 gas concentration  
 154 analyser on board.  $p\text{CH}_{4w}$  was determined from surface water methane concentrations (see above).  $K_0$  is the  
 155 methane solubility in  $\text{mol m}^{-3} \text{atm}^{-1}$  (Wiesenberg and Guinasso, 1979) and was calculated from temperature and  
 156 salinity obtained from corresponding CTD casts.  $k_{\text{ch}_4}$  is the methane gas transfer velocity in  $\text{m d}^{-1}$  which was  
 157 calculated using wind speed ( $U$ ), the Schmidt number ( $\text{Sc}_{\text{CH}_4}$ ) and the normalised gas transfer velocity ( $k_{660}$ )  
 158 according to (Wanninkhof, 2014):

$$159 \quad k_{\text{CH}_4} = 0.251 U^2 \left( \frac{\text{Sc}_{\text{CH}_4}}{660} \right)^{-0.5} \quad (5)$$

160 Wind speed was measured on board at 10 m above sea level. The Schmidt number describes the ratio between  
 161 kinematic viscosity of water and the gas diffusion coefficient, which relates the different  $k$ -values for different  
 162 gases (Jähne et al., 1987; Wanninkhof, 2014).

### 163 2.5 Statistical analysis

164 A principal component analysis (PCA) was carried out to study the relationship between environmental variables  
 165 and methanotrophic activity. The input variables for the PCA were temperature, salinity, density,  $k$ , MOx, and  
 166 dissolved methane concentrations. Prior to running the PCA, the variables were centered and scaled. We utilized  
 167 the R software and the ‘FactoMineR’ package (Lê et al., 2008) for the PCA analyses.

168 **3 Results**

169 **3.1 Dynamics of sea water properties**

170 Water column temperature varied between seasons and ranged from 6.3 °C to 24 °C (Fig. 2, Table 1). A clear  
 171 distinction could be made between colder seasons (autumn and winter) in which temperature ranged from 6.3 °C  
 172 to 9.1 °C and warmer (spring and summer) seasons where temperatures ranged from 14.2 °C to 24 °C. Water  
 173 temperatures at the reference station were similar in winter (6.9 °C) but colder in spring (10.5 °C) and summer  
 174 (20.3 °C) and warmer in autumn (11.8 °C) when compared to the Wadden Sea.

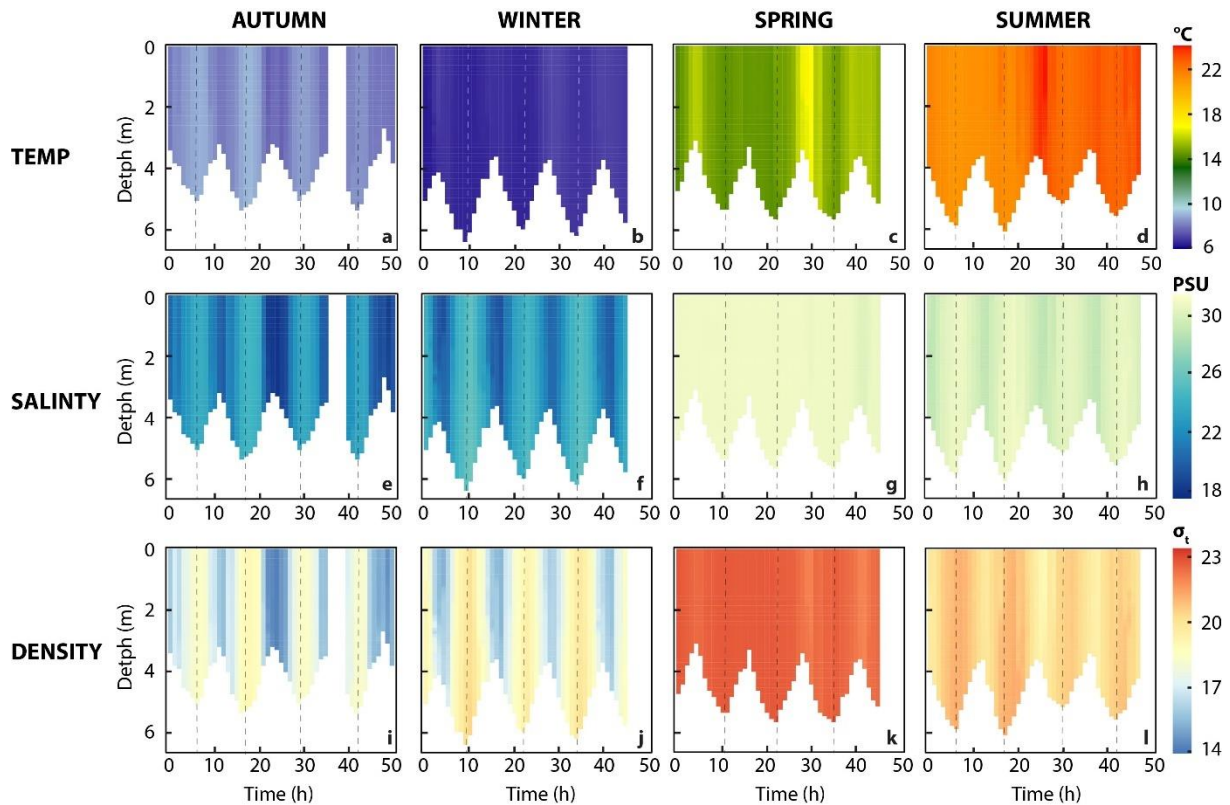
175 **Table 1.** Average seawater temperature, salinity, and density at the time-series station (central Dutch Wadden Sea) and  
 176 reference station (offshore Terschelling, North Sea). For the time-series station, values are presented as the mean  $\pm$  standard  
 177 deviation for the ~2 d measurement period during a given season. At the reference station, we only measured one CTD cast  
 178 per season.

	<b>Autumn</b>	<b>Winter</b>	<b>Spring</b>	<b>Summer</b>
<b>Temperature (°C)</b>	8.4 $\pm$ 0.4	6.7 $\pm$ 0.2	15.0 $\pm$ 0.6	22.1 $\pm$ 0.8
<b>Salinity (psu)</b>	22.4 $\pm$ 1.9	23.4 $\pm$ 1.8	31.3 $\pm$ 0.2	30.6 $\pm$ 0.6
<b>Density (<math>\sigma_t</math>)</b>	17.4 $\pm$ 1.4	18.3 $\pm$ 1.4	23.1 $\pm$ 0.2	20.8 $\pm$ 0.6
	<b>Autumn Ref st.</b>	<b>Winter Ref st.</b>	<b>Spring Ref st.</b>	<b>Summer Ref st.</b>
<b>Temperature (°C)</b>	11.8	6.8	10.4	20.0
<b>Salinity (psu)</b>	31.3	32.2	31.8	32.3
<b>Density (<math>\sigma_t</math>)</b>	23.7	25.2	24.4	22.7

179

180 On a diel scale, variation in water temperature were related to the tidal phase. In winter, spring, and summer,  
 181 maximum water temperatures were observed around low tide (LT, here defined as the time when we encountered  
 182 the lowest water depth during CTD casts, Fig. 2). This was 7.2 °C in winter, 17.3 °C in spring and 24.1 °C in  
 183 summer. Minimum water temperatures were around high tide (HT, high tide, here defined as the time when we  
 184 encountered maximum water depth during CTD casts, Fig. 2). This was 6.3 °C winter, 14.2 °C in spring, and 20.9  
 185 °C in summer. In autumn, this pattern was inverse with minimum water temperatures at LT (7.6 °C) and maximum  
 186 at HT (9.1 °C).

187 Like temperature, salinity differed strongly between colder (18 - 27 psu) and warmer seasons (29 - 32 psu; Fig. 2,  
 188 Table 1). Furthermore, salinity was higher during HT irrespective of season. Changes in density were caused by  
 189 salinity rather than temperature during all four seasons, with one exception in spring: after 28 hours of the time  
 190 series, salinity remained stable, but water temperatures decreased which lowered water density. Salinity levels at  
 191 the reference station in the North Sea were stable (31.3 – 32.3 psu) without obvious seasonal fluctuations.



192

193 **Figure 2.** Properties of sea water. (a-d) Spatiotemporal distribution of temperature, (e-h) salinity and (i-l) density. Dashed  
 194 line indicates high tide.

195 **3.2 Methane dynamics**

196 **3.2.1 Methane concentrations in the water column and in sediments**

197 Water column methane concentrations showed a high degree of variability and were clearly distinguishable  
 198 between the colder and warmer seasons (Fig. 3A-D, Table 2). We found a significant difference in average methane  
 199 concentrations between 1 m (16.0 nM) and 3 m (17.6 nM) water depth in winter ( $p \leq 0.007$ , Welch's t-test). In  
 200 autumn, methane concentrations were also lower at 1 m (15.5 nM) than at 3 m (16.2 nM) water depth, but the  
 201 difference was not significant. However, it is noteworthy that the methane concentrations at the beginning of the  
 202 time-series were around 35 nM and rapidly decreased to values below 15 nM within one day. During warmer  
 203 seasons, average methane concentrations were similar at the surface and in deeper waters, i.e. 40.9 nM (1 m) and  
 204 41.3 nM (3 m) in spring and 69.2 nM (1 m) and 69.4 (3 m) in summer. Methane concentrations at our reference  
 205 station were ~ 3 nM in winter, spring, and autumn and ~ 6 nM in summer and thus far lower when compared to  
 206 the Wadden Sea.

207 On a diel scale, methane concentrations varied during all seasons, roughly matching the tidal regime. In spring at  
 208 LT, depth-averaged methane concentrations were 42.6 nM, but decreased by ~ 25 % to 34.2 nM at HT. This pattern  
 209 also occurred in autumn where methane concentrations decreased by 21 % from 17.4 nM at LT to 14.4 nM at HT.  
 210 In winter (14.7 nM at LT and 14.3 nM at HT) and summer (72.5 nM at LT and 71.3 nM at HT), the difference  
 211 between LT and HT was smaller (Table 2).

212 Sediment methane concentrations increased with depth during all seasons (Fig. S1 in the Supplement).  
 213 Concentrations were similar in autumn (0.5 – 2.2  $\mu\text{M}$ ), winter (0.4 - 0.6  $\mu\text{M}$ ) and spring (0.5 - 0.9  $\mu\text{M}$ ) but in  
 214 summer, we found highly elevated sediment methane concentrations ranging from 3.6 to 18.7  $\mu\text{M}$ . The high  
 215 concentrations in sediments during the summer season are in line with an increase in dissolved methane  
 216 concentrations in the water column.

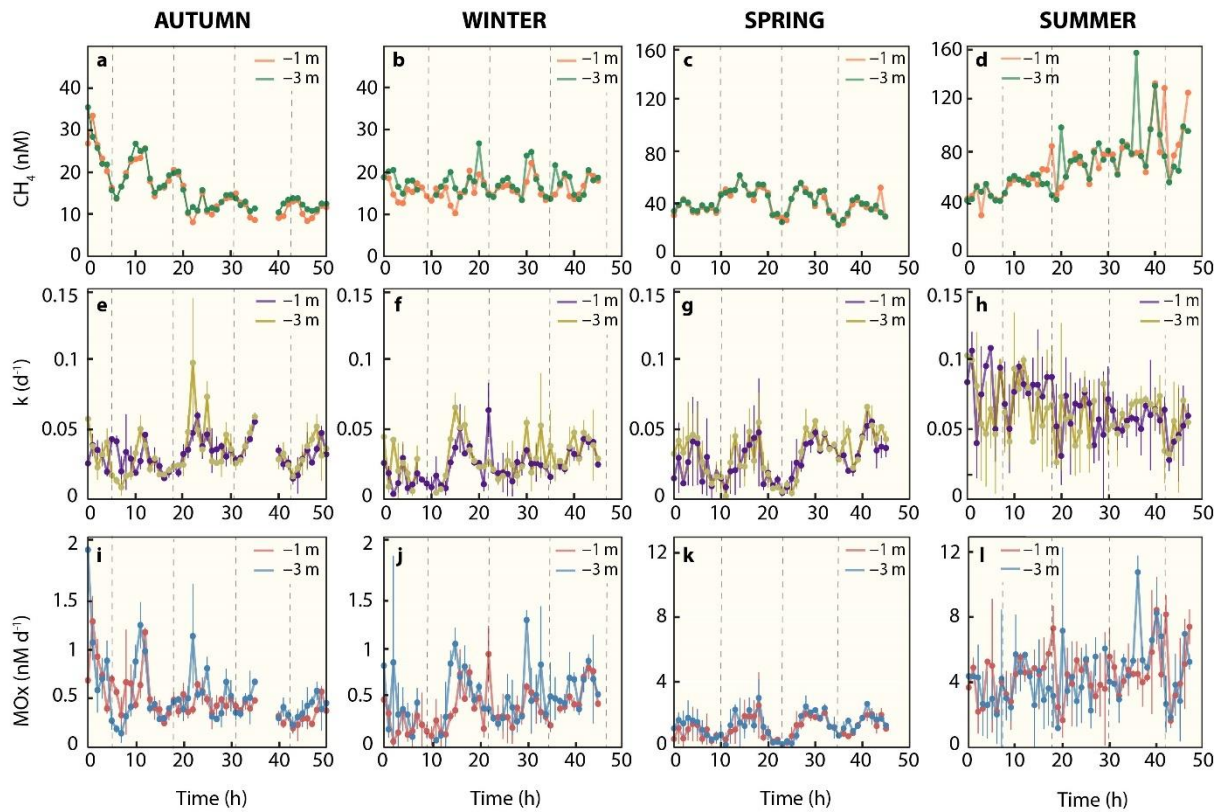
217

218  
219  
220  
221  
222  
223  
224

**Table 2. Methane dynamics in the Dutch Wadden Sea.** Average and standard deviation of methane concentrations,  $k$ ,  $MO_x$  and  $\delta D-CH_4$  during four seasons in 2019. Values represent averages for 1 and 3 m water depth (averaged over the two-day time series recorded for each season) as well as for low and high tide only (averaged over depth). LT = minimal water depth during CTD casts, HT = maximum water depth during CTD cast. Average wind speed and methane efflux to the atmosphere are averaged over the two-day time series recorded for each season. ns = not sampled. The reference station represents a single time point.

	Autumn	Winter	Spring	Summer
<b>Methane concentration (nM)</b>				
1 m water depth	15.5 ± 5.8	16.0 ± 2.4	40.9 ± 9.2	69.2 ± 21.4
3 m water depth	16.2 ± 5.7	17.6 ± 3.0	41.3 ± 8.9	69.4 ± 22.4
Low tide	17.4 ± 9.7	14.7 ± 2.1	42.6 ± 6.9	72.5 ± 36.1
High tide	14.4 ± 1.6	14.3 ± 0.6	34.2 ± 10.7	71.3 ± 27.4
Reference station	3.3	3.1	3.7	6.6
<b><math>k</math> (d<sup>-1</sup>)</b>				
1 m water depth	0.03 ± 0.01	0.02 ± 0.01	0.03 ± 0.01	0.07 ± 0.02
3 m water depth	0.03 ± 0.02	0.03 ± 0.01	0.03 ± 0.02	0.06 ± 0.02
Low tide	0.05 ± 0.01	0.03 ± 0.01	0.05 ± 0.01	0.08 ± 0.02
High tide	0.03 ± 0.01	0.03 ± 0.02	0.02 ± 0.01	0.06 ± 0.02
Reference station	0.01	0.0004	0.02	0.04
<b><math>MO_x</math> (nM d<sup>-1</sup>)</b>				
1 m water depth	0.48 ± 0.22	0.39 ± 0.21	1.16 ± 0.61	4.41 ± 1.49
3 m water depth	0.54 ± 0.34	0.52 ± 0.27	1.33 ± 0.71	4.33 ± 1.84
Low tide	1.05 ± 0.48	0.47 ± 0.24	2.02 ± 0.42	5.24 ± 2.33
High tide	0.50 ± 0.16	0.43 ± 0.31	0.59 ± 0.19	4.23 ± 2.13
Reference station	0.03	0.001	0.07	0.23
<b><math>\delta D-CH_4</math> (‰)</b>				
1 m water depth	-219 ± 31	ns	ns	-250 ± 17
3 m water depth	-224 ± 27	ns	ns	-250 ± 14
Low tide	-208 ± 41	ns	ns	-227 ± 1
High tide	-227 ± 13	ns	ns	-265 ± 3
<b>Methane sea-air flux (<math>\mu\text{mol m}^{-2} \text{d}^{-1}</math>)</b>				
Wind speed (m s <sup>-1</sup> )	8.0 ± 2.1	8.3 ± 1.4	7.9 ± 2.7	3.8 ± 1.6
Methane flux	40.2 ± 28.1	38.7 ± 14	144.8 ± 98	72.9 ± 52
Atmosphere conc. (ppm)	2.0 ± 0.03	2.12 ± 0.19	2.02 ± 0.15	2.14 ± 0.15

225



226

227 **Figure 3.** Methane dynamics. (a-d) Dissolved methane concentration, (e-d) first-order rate constant, (i-l) methane oxidation  
 228 rates. Note that for dissolved methane concentrations in colder seasons, autumn and winter, the y-axis differs from warmer  
 229 seasons, spring, and summer. Dashed line indicates high tide.

### 230 3.2.2 Methane oxidation rates

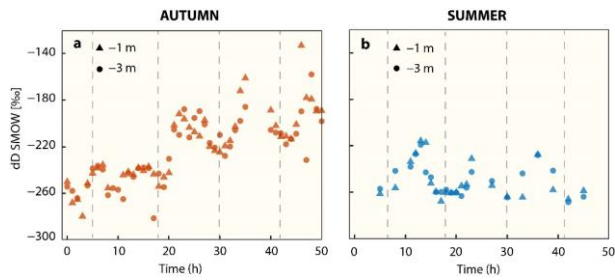
231 Similar to methane concentrations, we observed strong seasonal differences in MOx (Fig. 3I-L, Table 2). Depth-  
 232 averaged MOx in spring (1.2 nM d<sup>-1</sup>) and summer (4.4 nM d<sup>-1</sup>) was ~ 3 and ~ 9 – fold higher than in winter (0.5  
 233 nM d<sup>-1</sup>) and autumn (0.5 nM d<sup>-1</sup>). MOx at 1 m and 3 m water depth statistically differed from each other in winter  
 234 ( $p \leq 0.01$ , Welch's t-test), but not in spring, summer, and autumn. MOx at the reference station was < 5 % of MOx  
 235 in the Wadden Sea, with maxima found in summer (0.2 nM d<sup>-1</sup>).

236 On a diel scale, MOx showed fluctuations during all seasons. In general, depth-averaged MOx was higher during  
 237 LT compared to HT. In autumn average MOx at LT (0.79 nM d<sup>-1</sup>) was about 2 – fold higher and significant different  
 238 from MOx at HT (0.38 nM d<sup>-1</sup>,  $p \leq 0.03$ , Welch's t-test).

239 In winter, the difference between MOx at LT (0.47 nM d<sup>-1</sup>) and HT (0.43 nM d<sup>-1</sup>) was small. In spring, depth-  
 240 averaged MOx at LT (2.02 nM d<sup>-1</sup>) was about 4 – fold and significantly ( $p \leq 6.4 \times 10^{-6}$ , Welch's t-test) higher than  
 241 during HT (0.58 nM d<sup>-1</sup>). In summer, MOx was high at both, LT (5.2 nM d<sup>-1</sup>) and HT (5.4 nM d<sup>-1</sup>). Similarly,  $k$   
 242 was substantial higher (16 – 63 %) at LT than HT in all seasons (Fig. 3E-H, Table 2). In fact, the difference in  
 243 depth-averaged  $k$  between LT and HT was significant in autumn ( $p \leq 0.003$ , Welch's t-test) and spring ( $p \leq 6 \times$   
 244  $10^{-5}$ , Welch's t-test, Table S1 in the Supplement).

### 245 3.2.3 Stable hydrogen isotope signatures

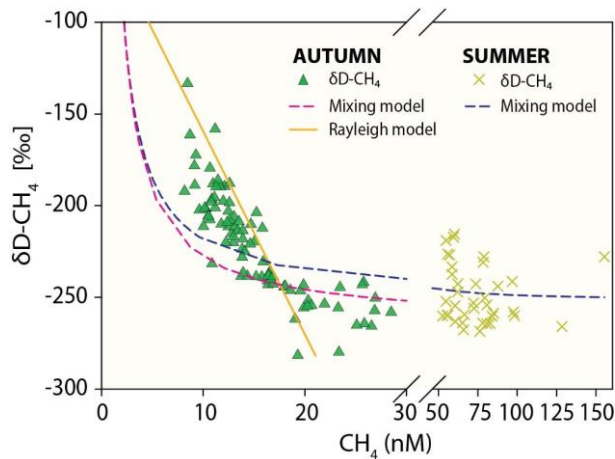
246 The stable hydrogen isotope composition of dissolved methane was only measured in autumn and summer (Fig.  
 247 4, Table 2). In autumn, average  $\delta D-CH_4$  over the entire time-series was -219 ‰ at 1 m water depth and -224 ‰  
 248 at 3 m water depth, but there was a generally strong trend towards higher  $\delta D-CH_4$  values over the two-day period  
 249 from about -260 ‰ to about -180 ‰. In summer the mean  $\delta D-CH_4$  values were homogenous throughout the water  
 250 column (-250 ‰) and generally lower than in autumn. Except for the first full tidal cycle in autumn, the results  
 251 showed a tidal imprint on  $\delta D-CH_4$  values with higher  $\delta D-CH_4$  values at LT and lower values at HT independent  
 252 of depth and season (Fig. 4).



253

254 **Figure 4.** Progression of  $\delta\text{D-CH}_4$  signatures in (a) autumn and (b) summer at 1 m and 3 m water depth. Vertical dashed line  
 255 indicates high tide.

256 In addition to tidal patterns, the  $\delta\text{D-CH}_4$  values in autumn were substantially higher at lower methane  
 257 concentrations ( $< 21$  nM, Fig. 5). Linear mixing alone of (i) well-mixed surface waters in equilibrium with  
 258 atmospheric methane and (ii) the maximum methane concentration in the water column, both concentrations with  
 259 their associated isotopic signatures, would result in concentration/isotope data as depicted by the mixing lines in  
 260 Fig. 5. Results in autumn clearly deviated from this mixing line at low methane concentrations. On the other hand,  
 261 the open system Rayleigh fractionation model that we ran for low methane concentration in autumn yielded an  $\epsilon$ -  
 262 value of  $-97$  ‰ and matched the steep rise in  $\delta\text{D-CH}_4$  with decreasing methane concentration much better ( $R^2 =$   
 263  $0.79$ ). This directly indicates that  $\text{MOx}$  is the dominant mechanism driving  $\delta\text{D-CH}_4$  to higher values at low  
 264 concentrations.



265

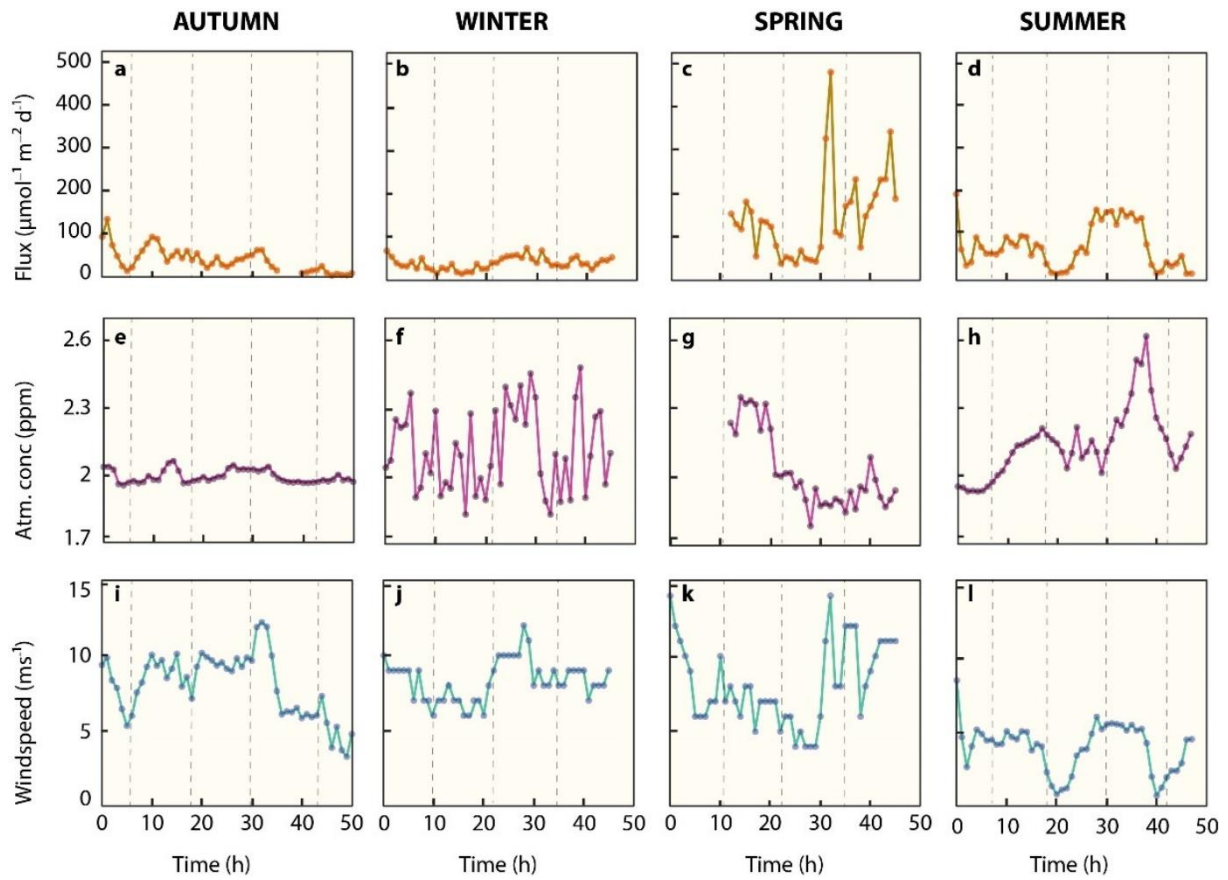
266 **Figure 5.** Methane concentration versus  $\delta\text{D-CH}_4$  - mixing and oxidative removal in autumn and summer. Dashed lines show  
 267 methane concentration/isotope dynamics determined with a two-endmember mixing model considering (i) well-mixed Wadden  
 268 Sea surface waters and (ii) methane charged waters as endmembers. Methane concentration and stable hydrogen isotope  
 269 composition following oxidative removal according to a Rayleigh model for low methane concentrations are depicted as a solid  
 270 line. Samples with methane concentrations  $< 21$  nM ( $\delta\text{D-CH}_4 = \sim -217$  ‰) in autumn and  $< 61$  nM ( $\delta\text{D-CH}_4 = \sim -244$  ‰) in  
 271 summer were defined as the methane source signal and thus starting point of the Rayleigh fractionation model. The apparent  
 272 isotope enrichment ( $\epsilon$  see also Fig. S2 in the Supplement) was  $-97$  ‰ in autumn with an  $R^2$  of  $0.79$ . Neither the mixing nor the  
 273 Rayleigh model are well constrained for  $\delta\text{D-CH}_4$  in summer; the mixing line is thus only shown for comparison and  $\epsilon$  could  
 274 not be calculated.

### 275 3.2.4 Diffusive efflux to the atmosphere

276 The water column in the Wadden Sea was consistently methane supersaturated ( $> 8$  nM) with respect to  
 277 atmospheric equilibrium ( $\sim 2.6$  nM) during all sampling campaigns (Fig. 3, Table 2), which indicates a continuous  
 278 release of methane from the water to the atmosphere throughout the measurement series. Atmospheric  
 279 concentrations were similar ranging from 1.8 to 2.6 ppm, with relatively constant concentrations in autumn and  
 280 more erratic concentrations in winter, spring, and summer (Fig. 6e-h, Table 2). Noteworthy is the sharp increase  
 281 of atmospheric methane from 2 to 2.6 ppm between 29 and 38 hours in summer before decreasing again to 2 ppm.

282 Windspeeds in autumn, winter, and spring were relatively high (typically  $> 5$   $\text{ms}^{-1}$ ) when compared to calmer  
 283 conditions in summertime (typically  $< 5$   $\text{ms}^{-1}$ , Fig. 6i-l, Table 2). As a result of the strong but variable wind forcing,  
 284 diffusive methane fluxes fluctuated in magnitude within, and between season (Fig. 6a-d, Table 2). Average  
 285 diffusive fluxes in autumn and winter were with  $< 40$   $\mu\text{mol m}^{-2} \text{d}^{-1}$  about 4 – fold lower than in spring and 2 – fold  
 286 lower than in summer. Maximum efflux ( $479$   $\mu\text{mol m}^{-2} \text{d}^{-1}$ ) in spring occurred after the wind velocity increased

287 rapidly from  $6 \text{ m s}^{-1}$  to  $14 \text{ m s}^{-1}$  within two hours and methane concentrations slightly increased from 38 nM to 45  
288 nM.



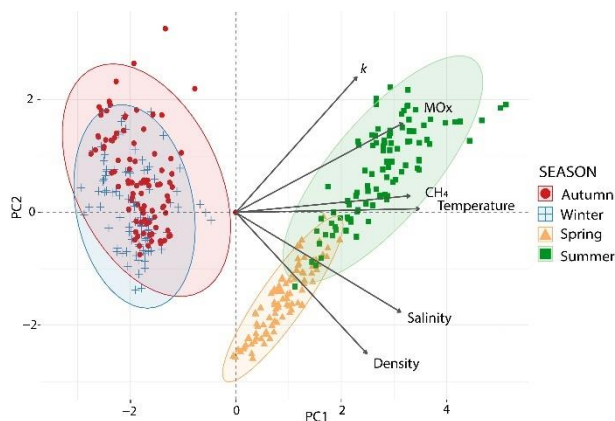
289

290 **Figure 6.** Diffusive methane flux. (a-d) Sea surface atmosphere methane fluxes, (e-h) Seasonal atmospheric methane  
291 concentrations, (i-l) local wind speed. Vertical dashed lines indicate high tide.

292

### 293 3.3 Statistical Analysis

294 To study the relationship between environmental variables and methanotrophic activity, we conducted a Principal  
295 Component Analysis (PCA). The outcome explained 92 % of the data variability on the first two components (Fig.  
296 7, Table S2 in the Supplements). The main gradient (PC1: 69 %) showed a contrast between autumn/winter and  
297 summer and spring. Temperature, salinity, methane concentrations and MO<sub>x</sub> peaked in summer and spring, while  
298 lower values were measured in winter/autumn. The relatively small ellipse in spring indicates that samples show  
299 more similarity than in other seasons. The second gradient distinguished the spring samples from the summer  
300 samples, with higher k values observed in summer and greater density in spring (PC2: 23 %).



301  
302 **Figure 7.** Principal Component Analysis (PCA) of environmental conditions across seasons in the Dutch Wadden Sea. Biplot  
303 of a PCA of the explanatory variables as vectors (in black) and observations (marks) of each season on the first (x-axis, PC1)  
304 and second principal component (y-axis, PC2). Coloured concentration ellipses (size determined by a 0.95-probability level)  
305 show the observations grouped by season. The magnitude of the vectors (line length) shows the strength of their contribution  
306 to the PCs. Vectors pointing in similar directions indicate positively correlated variables and vectors at angles > 90° indicate  
307 no correlation.

## 308 4 Discussion

309 The Wadden Sea is a highly productive ecosystem (Philippart et al., 2009) where the decay of organic matter  
310 supports high rates of methanogenesis in sediments (Røy et al., 2008; Wu et al., 2015), Which in return leads to  
311 high methane concentrations in the Wadden Sea's water column (Grunwald et al., 2007; Grunwald et al., 2009).  
312 Little knowledge, however, exists on the variability of methane dynamics on short time scales of hours to days or  
313 between seasons and the underlying controls on this variability. Here, we measured water column methane  
314 concentrations, methane oxidation and the oceanographic regime as well as atmospheric methane mixing ratios  
315 and wind velocity in the Dutch sector of the Wadden Sea for two days during four consecutive seasons in 2019.

### 316 4.1 Water column properties

317 In general, we found a clear distinction between colder (autumn and winter) and warmer (spring and summer)  
318 seasons (Figs. 2, 7). North Sea waters with incoming tide, flow through tidal inlets that in turn branch into  
319 successively smaller tidal creeks in which water-flow direction alternates with the tidal phase. This then led to  
320 increasing water temperatures in autumn but decreasing water temperatures in winter. The high temperature of  
321 Wadden Sea waters during incoming tide in autumn can be explained by the fact that the shallow Wadden Sea  
322 cools rapidly once the summer is over, while the North Sea's large water volume takes longer to cool down.

323 Salinity levels were on average lower in colder seasons compared to warmer seasons, likely because land runoff  
324 and ground water discharge are typically higher in autumn and winter because of the overall higher precipitation  
325 levels during the cold seasons (Van Aken, 2008). A higher level of freshwater inflow from land was also evident  
326 from the rapidly dropping salinity levels during falling and LT in autumn and winter (Fig. 2). This freshening  
327 effect is amplified at times when the Dutch Ministry of Infrastructure and Water management (Rijkswaterstaat)  
328 opens water gates to discharge excess water from lake IJssel (Fig. 1), which occurs more often in colder seasons  
329 due to increased input of precipitation, groundwater discharge as well as surface and riverine discharge to the lake.  
330 During the warmer and dryer seasons, water gates are mostly kept closed to ensure that the lake's water level stays  
331 high. However, freshwater inflow into the Wadden Sea was evident during all seasons because incoming North  
332 Sea water generally increased salinity levels at HT independent of sampling time. The North Sea water mass  
333 entering the Wadden Sea during incoming tide hence becomes overprinted in the Wadden Sea area as a result of  
334 mixing with waters from terrestrial sources.

#### 335 **4.2 Differences in methane concentrations and isotopic signatures on time scales of seasons**

336 Sediment and water column methane concentrations were highly elevated in summer (Figs. 3, S1 in the  
337 Supplement and Table 2). In fact, average sediment methane concentrations increased 17 – fold in summer  
338 compared to spring two months earlier. This increase is probably related to the remineralization of the spring  
339 phytoplankton bloom that takes place in the months of April and May (Philippart et al., 2009) leading to elevated  
340 rates of methanogenesis in anaerobic sediments (Beck and Brumsack, 2012). A time lag of one to two months  
341 between the peak of the spring bloom and methane release from sediments was also observed in the Baltic Sea  
342 (Bange et al., 2010). In the Wadden Sea, where sediments are generally silty and organic-rich, it is likely that  
343 temperature plays a crucial role in controlling methanogenesis, in addition to the elevated inputs of organic matter.  
344 As water temperatures increase towards summer, microbial methanogenesis in the sediments is further enhanced  
345 (Yvon-Durocher et al., 2014; Borges et al., 2018). We indeed observed lower methane concentrations in autumn  
346 and winter compared to spring and summer, which is most likely related to both reduced organic matter input and  
347 colder temperatures. It has to be noted that the sediment methane concentrations presented here are comparably  
348 low as sediment methane concentrations close to saturation levels were previously found at other locations in  
349 Wadden Sea sediments (Røy et al., 2008; Wu et al., 2015). We did not measure sulphate concentrations, but the  
350 methane profiles indicate that we only reached the upper part of the methane-sulphate transition zone below of  
351 which methanogenesis proceeds. Also, sediment methane concentrations can be variable on spatial scales of  
352 metres. Depending on the hydrographic regime, the methane-sulphate transition zone can be metres below the tidal  
353 flat sediments (Wu et al., 2015), but pore water flow can also transport reduced compounds such as sulphide and  
354 methane to the sediment surface (Røy et al., 2008).

355 Methane release from sediments and the relatively low wind speed (and thus relatively low forcing to drive  
356 diffusive efflux) in summer led to charging of the water column with methane. MOx discriminates against  
357 isotopically heavy methane and thus causes an isotopic enrichment of residual methane. The isotopic  
358 discrimination effect manifests more pronouncedly at low methane concentrations. Indeed, we found more  
359 pronounced MOx induced isotopic discrimination effects in autumn at low methane concentrations (< 21 nM). At  
360 higher methane concentrations (> 21 nM) values were more depleted and were comparable to summer  $\delta D-CH_4$   
361 values. We relate the  $\delta D-CH_4$  values (~ -217 ‰ in autumn and ~ -244 ‰ in summer) at higher methane  
362 concentrations (> 21 nM in autumn and > 61 nM in summer) to the  $\delta D-CH_4$  source signal (Fig. 4A, 5). At these  
363 concentrations, the isotope effect imposed by MOx is masked by the high background methane and/or is  
364 overprinted by methane entering the water column from sediments.

#### 365 **4.3 Differences in MOx on seasonal time scales**

366 The activity of MOBs in the water column is determined by the availability of methane, oxygen, nutrients, and the  
367 size of the standing stock of the MOB community (Reeburgh, 2007; Crespo-Medina et al., 2014; Steinle et al.,  
368 2015). The Wadden Sea water column is a nutrient rich and typically oxygenated environment, we hence argue  
369 that nutrient and O<sub>2</sub> availability are not a limiting factor for MOB activity. However, MOBs in the Wadden Sea  
370 need to cope with high fluctuations in temperature, salinity, and methane availability (see above).

371 We did not measure the size of the MOB community; nevertheless, it seems likely that the highly variable water  
372 column properties with admixture of different water masses and resuspension of particles effects the standing stock  
373 of the MOB community and/or its activity. Notably, North Sea waters with potentially low MOB standing stock  
374 (indicated by the low k value at the reference station) enter the Wadden Sea during incoming tides. As these waters  
375 traverse through the Wadden Sea, they acquire methane and likely carry microbes irrigated from sediments  
376 and/or originating from mixing with terrestrial waters; incoming North Sea waters hence undergo oceanographic (see  
377 above) and biogeochemical overprinting. On short time scales, microbes carried with the tidal current through the  
378 Wadden Sea will consequently be exposed to variable conditions regarding salinity and temperature levels, and  
379 methane concentration.

380 Previous studies showed that elevated salinity often led to an immediate decrease in MOx in terrestrial/lacustrine  
381 systems (Ho et al., 2018; Zhang et al., 2023). Likewise, marine methanotrophs seem to function best at salinity  
382 levels of > 20 psu (Osudar et al., 2017), while a sudden decrease in salinity can strongly inhibit MOx (Hirayama  
383 et al., 2013; Tavormina et al., 2015). This begs the question if waters, with rapidly changing salinity levels such  
384 as the Wadden Sea, are environments that are rather not conducive for MOx, in particular in colder months where  
385 salinity levels may drop to ~ 20 psu because of elevated freshwater influx (see above). While MOx was indeed  
386 lower in autumn and winter, the relative decrease in MOx was moderate in comparison to the previous literature  
387 findings (Osudar et al., 2017; Zhang et al., 2023). Also, autumn and winter are colder and defined by lower methane

388 levels, which likely reduces MOx further. Across seasons, the PCA (Fig. 7), and Pearson correlation coefficients  
389 of pairs of variables (Fig. S3 in the Supplement) indicated that MOx (or  $k$ ) and salinity (or density) are not or only  
390 weakly correlated. The Wadden Sea thus seems to host a euryhaline MOB community that contrast with MOB  
391 communities from terrestrial/lacustrine (Zhang et al., 2023) and oceanic origin (Osudar et al., 2015), which seem  
392 less able to cope with varying salinity levels.

393 Sediments and the water column in the Wadden Sea are increasingly fuelled with methane when ambient  
394 temperatures rise. The higher availability of methane could then enhance methanotrophic activity (Reeburgh,  
395 2007). Indeed, we found a seasonal imprint with highest MOx levels in summer that were 3-fold higher than those  
396 observed in spring, 9-fold higher than in autumn and 10-fold higher than in winter (Table 2). A correlation between  
397 methane, temperature and MOx was also apparent from the PCA (Figs. 7, S3 in the Supplement). We note that not  
398 only MOx, but also the first order rate constant  $k$  was stimulated by higher methane concentrations (MOx is a  
399 function of  $k$  and  $[\text{CH}_4]$ , see eq. 3) and temperature. A positive effect of methane on MOx and  $k$  is often associated  
400 with changes in methane concentrations over several orders of magnitude (Crespo-Medina et al., 2014; James et  
401 al., 2016). Here we found that  $k$  doubled in summer compared to spring, while methane concentrations were only  
402 30 nM higher, i.e., 1.7-fold. This suggests that a combination of methane availability and temperature determined  
403  $k$  in our study. I.e., the MOB's may have been stimulated on the enzymatic level. However, the fact that  $k$  remained  
404 stable in colder seasons with low water temperatures, suggest that additional factors, likely MOB community size  
405 (Steinle et al., 2015), might play a more important role in maintaining  $k$ . For example, MOB's from sediments can  
406 be resuspended into the water column due to tidal currents, or transported from sediments to the water-column  
407 with bubbles as has been found at other cold seeps (Steinle et al., 2016; Jordan et al., 2020; Jordan et al., 2021).  
408 Resuspension could thus be a key driver of the Wadden Sea water column MOB communities, with major  
409 consequences for maintaining a microbial filter under less favourable conditions.

#### 410 **4.4 Methane dynamics on times scales of hours to days.**

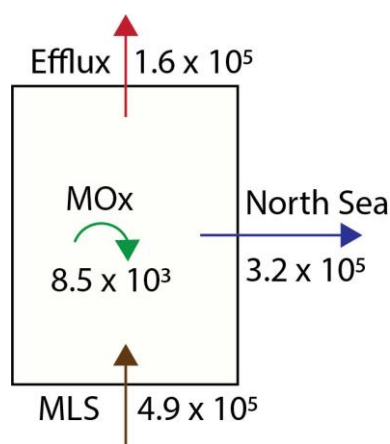
411 Strong hydraulic dynamics are an important characteristic of the Dutch Wadden Sea, with tidal currents  
412 interchanging a large water volume with the North Sea twice per day (Gräwe et al., 2016). With the change in tidal  
413 phase, the hydrostatic pressure changes rapidly with water depth, which triggers porewater flow (tidal pumping,  
414 Røy et al., 2008; Santos et al., 2015)) but may also trigger expansion and ebullition of gas bubbles (Schmale et  
415 al., 2015; Jordan et al., 2020). Similar effects are caused by tidal currents flowing over bathymetric features, which  
416 triggers pore water flow, too, and additionally resuspends sediments and MOB's into the water column (Bussmann,  
417 2005; Abril et al., 2007; Røy et al., 2008). On the other hand, incoming water from the open North Sea contains  
418 relatively low amounts of methane (<6 nM as measured at our reference station), hence, this will dilute the Dutch  
419 Wadden Sea's methane content, and outflowing water will export methane from the Dutch Wadden Sea main  
420 water body.

421 Temporal patterns of methane concentration and MOx indeed correlated well with tidal oscillation (Figs. 3, S1 in  
422 the Supplements, Table 2). Independent of the seasons, methane concentrations and MOx were elevated at LT.  
423 The tidal effect seemed most pronounced in spring where at LT, methane concentrations (1.3 – fold),  $k$  (2.5 – fold)  
424 and MOx (4 – fold) were higher than at HT, independent of depth. We found it surprising that, just like methane  
425 concentrations,  $k$  also was substantially higher during LT compared to HT independent of seasons and despite an  
426 overall lower salinity at low tide (Figs. 3, S1 in the Supplement, Table 2). To the best of our knowledge, this has  
427 not been described before. It seems unlikely that the MOB community substantially grew or that the velocity of  
428 the MOB's metabolism increased/decreased in a time frame of a few hours. We rather argue that the observed  
429 oscillation is caused by a likewise oscillation of shear force and hydrostatic pressure, leading to resuspension of  
430 MOB's from sediments as well as elevated release of methane from the sea floor.

431 Grunwald et al. (2007 and 2009) conducted time-series measurements in the German sector of the Wadden Sea  
432 near the island of Spiekeroog. There, absolute methane concentrations were ~ 3 – fold higher in spring and summer  
433 and ~ 15 – fold higher in winter when compared to our study. This might be related to local factors, for example  
434 the vicinity of the estuaries of the rivers Eems and more importantly Weser close by Spiekeroog, which increase  
435 the background methane concentrations in this sector of the Wadden Sea. Like in our study, Grunwald et al. (2007,  
436 2009) also reported on a strong influence of tides, with highest methane concentrations at low tide, probably related  
437 to tidal pumping, while inflowing waters showed concentrations typical for the open North Sea in the German  
438 Bight. The temporal aspects and processes determining methane dynamics discussed in our work are thus not a  
439 local feature but applicable to the entire Wadden Sea and likely to other mud flat areas influenced by tides, too.

#### 440 4.5 Methane emissions from the Dutch Wadden Sea

441 Surface waters were supersaturated in methane with respect to the atmospheric equilibrium during all seasons; the  
442 Wadden Sea is consequently a constant source of methane to the atmosphere. Just as for dissolved methane  
443 concentrations and MOx, methane efflux to the atmosphere was higher during warmer seasons compared to colder  
444 seasons. This was primarily driven by methane concentrations rather than wind velocity: wind speeds were similar  
445 in autumn, winter, and spring, but 2-fold higher methane concentrations in spring translate to a 4-fold higher sea-  
446 air flux when compared to autumn and winter. In summer, meteorological conditions were dominated by a heat  
447 wave with extremely low wind speeds. This resulted in a comparably low methane efflux to the atmosphere  
448 (though still higher than during the colder seasons) leading to an accumulation of methane in the water column.  
449 Previously described diffusive methane fluxes at coastal systems vary over several orders of magnitude and appear  
450 site specific. For instance, at the Baltic sea coast, fluxes of up to  $15 \mu\text{mol m}^{-2} \text{d}^{-1}$  have been reported (Bange et al.,  
451 2010; Steinle et al., 2017), while in arctic shelf seas, diffusive fluxes of up to  $240 \mu\text{mol m}^{-2} \text{d}^{-1}$  were found  
452 (Thornton et al., 2016). In the Southern bight of the North Sea, reported fluxes at the coast were up to  $345 \mu\text{mol m}^{-2} \text{d}^{-1}$   
453 ( $\text{Borges et al., 2018}$ ). In comparison, estuarine research along the European Atlantic coast found a median  
454 flux of  $130 \mu\text{mol m}^{-2} \text{d}^{-1}$  (Middelburg et al., 2002), which is similar to the fluxes that we found in the Dutch  
455 Wadden Sea ( $\sim 39$  to  $145 \mu\text{mol m}^{-2} \text{d}^{-1}$ ). Globally, tidal flats were estimated to emit  $\text{CH}_4$  at a median rate of  $\sim 3.6$   
456  $\text{mg m}^{-2} \text{d}^{-1}$  ( $226 \mu\text{mol m}^{-2} \text{d}^{-1}$ ; (Rosentreter et al., 2021)), which is similar (1.5 to 6-fold higher) than our flux  
457 estimates from the Wadden Sea.



458

459 **Figure 8.** Methane budget for the Dutch Wadden Sea is calculated based on values for the Wadden Sea's geometry, tidal  
460 displacement volume, and biogeochemical parameters as discussed in the text. MLS stands for methane liberation from  
461 sediments. All values are presented as  $\text{mol CH}_4 \text{d}^{-1}$ .

462 Towards a roughly estimated methane budget for Dutch Wadden Sea, we combined our diffusive flux, MOx and  
463 methane concentration data (Fig 8.) as well as estimates of the Wadden Sea water volume and tidal prism. Our  
464 flux estimates (Table 2) translate to an annual average sea surface-atmosphere flux of  $74 \mu\text{mol m}^{-2} \text{d}^{-1}$ .  
465 Extrapolating this to the area of Dutch sector of the Wadden Sea ( $\sim 2200 \text{ km}^2$ ; (Materić et al., 2022) implies that  
466  $1.6 \times 10^5 \text{ mol CH}_4 \text{d}^{-1}$  escapes from the Dutch Wadden Sea to the atmosphere (Table 2). The average water volume  
467 of the Dutch Wadden Sea is about  $5.15 \text{ km}^3$  (Materić et al., 2022); hence the annual average of  $1.7 \text{ nM d}^{-1}$  of MOx  
468 translates to  $0.09 \times 10^5 \text{ mol CH}_4 \text{d}^{-1}$  that is oxidized in the water column by MOBs. In addition to atmospheric  
469 efflux and microbial consumption, methane rich waters are also flushed into the North Sea. To estimate this, we  
470 simplified that the total tidal prism of  $4.5 \text{ km}^3$  (Gräwe et al., 2016) is an approximation of the net amount of water  
471 that leaves the Wadden Sea during LT. With respect to our measured mean methane concentration ( $36.8 \text{ nM}$ ),  
472 about  $1.6 \times 10^5 \text{ mol}$  of methane are thus flushed towards the North Sea twice daily, i.e.,  $3.2 \times 10^5 \text{ mol per day}$ . A  
473 large uncertainty in this calculation is caused by the delay of  $\sim 3$  hours in tidal phases between the Western and  
474 Eastern part of the Dutch Wadden Sea. In other words, methane-rich waters are flowing out of the tidal inlet in the  
475 West can be entrained in the current that starts flowing back into the Wadden Sea at eastern tidal inlets. Therefore,  
476 the net loss of methane to the Wadden Sea is probably lower than described above. Still, data from our reference  
477 station show only slightly oversaturated methane concentrations ( $< 6 \text{ nM}$ ) suggesting that the amount of methane  
478 flowing back into the Wadden Sea is rather low. A similar observation was found during a tidal inlet study in the  
479 German Wadden Sea (Grunwald et al., 2009). Though overall methane concentrations were higher, methane  
480 concentrations in North Sea waters flowing into the Wadden Sea were 60 % lower compared to waters flowing  
481 out of the Wadden Sea at low tide. Excluding allochthonous methane sources (for example methane influx with

482 freshwater from Lake IJssel), the Dutch Wadden Sea's methane budget must be supported by a total rate of  
483 methanogenesis that at least equals the sum of methane efflux to the atmosphere, water column methanotrophy  
484 and methane outflow to the North Sea; together these amount to  $4.9 \times 10^5 \text{ mol d}^{-1}$ . This is comparable to  
485 methanogenesis rates in the Eckernförde Bay in the Baltic Sea in the Baltic Sea (Maltby et al., 2018). Note that  
486 this accounts for the amount of methane liberated from sediments, while it neglects methane oxidation in sediments  
487 (dominantly anaerobic oxidation of methane), which can retain a substantial fraction of methane in sediments  
488 (Reeburgh, 2007). Hence, the total rate of methanogenesis in the Wadden Sea is consequently much higher.

489 Taken all methane export terms/sinks considered together (MOx, efflux and tidal displacement amounting to  $4.9$   
490  $\times 10^5 \text{ mol d}^{-1}$ ), MOx reduces roughly 2 % of the Wadden Sea's methane budget, while about 1/3<sup>rd</sup> of methane  
491 escapes to the atmosphere and the remaining  $\sim 2/3^{\text{rd}}$  is flushed into the North Sea (where it may be further oxidised  
492 and/or released to the atmosphere). The effect of MOx on the Wadden Sea's methane budget is low when compared  
493 to the global ocean, where an estimated  $>90$  % of water column methane is consumed by MOx (Reeburgh, 2007).  
494 As the Wadden Sea is very shallow, liberation of methane from sediments to the atmosphere is fast; in other words,  
495 MOBs have a very limited time to consume methane released from the sediments before it is liberated to the  
496 atmosphere or flushed with tides to the North Sea. In a meta study, Rosentreter et al. (2021) estimated a global  
497 median methane efflux from tidal flats (covering  $\sim 128000 \text{ km}^2$  globally; (Murray et al., 2019)), to the atmosphere  
498 of  $0.17 \text{ Tg y}^{-1}$ . We found a total annual diffusive sea-air flux from the Dutch sector of the Wadden Sea (2200 km<sup>2</sup>)  
499 of  $\sim 0.001 \text{ Tg y}^{-1}$ , which alone already accounts for 0.6 % of the global methane emissions from tidal flats to the  
500 atmosphere.

## 501 **5 Summary and conclusion.**

502 Our work revealed substantial variations in methane dynamics when comparing colder and warmer seasons; in  
503 warmer seasons, methane concentrations, efflux and MOx were higher compared to colder seasons. Still during  
504 colder seasons waters were continuously supersaturated with methane and higher wind speeds in these seasons led  
505 to substantial amounts of methane released to the atmosphere. We show that tidal dynamics are a key control for  
506 methanotrophic activity and methane distribution. Although changing water column properties and methane  
507 concentrations do not provide continuity, the capacity of the microbial methane filter is seemingly stable, with an  
508 active MOB community even under unfavourable conditions. Nevertheless, MOx only consumes a minor fraction  
509 of the methane inventory of the highly dynamic Wadden Sea, while most is or liberated to the atmosphere and  
510 flushed out with tidal currents into the neighbouring North Sea. It appears likely that the contribution of the  
511 Wadden Sea to the global atmospheric methane budget will alter in the future due to global warming, and changes  
512 in nutrient availability and more frequently occurring storm events. Our results finally highlight the importance of  
513 repeated high frequency sampling strategies in dynamic coastal waters to resolve temporal patterns on diel and  
514 seasonal scales.

515 *Data availability.* All data will be archived and made publicly available in the data base DAS (Data Archive  
516 System, [www.nioz.nl/en/research/dataportal/das](http://www.nioz.nl/en/research/dataportal/das)).

517  
518 The supplement related to this article is available online.  
519

520 *Author contributions.* The study was designed by Tim de Groot, Thomas Röckmann, and Helge Niemann. On-  
521 board sampling was performed by Tim de Groot, Anne Mol, Katherine Mesdag, Julia Engelmann, Pierre Ramond,  
522 and Helge Niemann. Further geochemical analysis was conducted by Tim de Groot, Anne Mol, Katherine Mesdag,  
523 and Rachel Ndhlovu. Microbial rates were measured by Tim de Groot and Anne Mol. Statistical analysis was  
524 carried out by Tim de Groot and Pierre Ramond. Helge Niemann supervised the research project. The manuscript  
525 was prepared by Tim de Groot with input from all authors.

526 *Competing interests.* The authors disclose that at least one of the (co-)authors holds a position on the editorial  
527 board of Biogeosciences.

528  
529 *Acknowledgements.* Our gratitude goes to the captain and crew of R/V Navicula, as well as the staff of the  
530 geochemical, radioisotope, and atmospheric laboratories at NIOZ and IMAU, for their exceptional support. We  
531 would also like to extend our appreciation to Eric Wagemaakers for regularly calibrating the CTD.

## 532 **References**

533 Abril, G., Commarieu, M.-V., and Guérin, F.: Enhanced methane oxidation in an estuarine turbidity maximum,  
534 *Limnology and Oceanography*, 52, 470-475, <https://doi.org/10.4319/lo.2007.52.1.0470>, 2007.

535 Bange, H. W., Bartell, U. H., Rapsomanikis, S., and Andreae, M. O.: Methane in the Baltic and North Seas and a  
536 reassessment of the marine emissions of methane, *Global Biogeochemical Cycles*, 8, 465-480,  
537 <https://doi.org/10.1029/94GB02181>, 1994.

538 Bange, H. W., Bergmann, K., Hansen, H. P., Kock, A., Koppe, R., Malien, F., and Ostrau, C.: Dissolved methane  
539 during hypoxic events at the Boknis Eck time series station (Eckernförde Bay, SW Baltic Sea), *Biogeosciences*,  
540 7, 1279-1284, 10.5194/bg-7-1279-2010, 2010.

541 Barker, J. F. and Fritz, P.: Carbon isotope fractionation during microbial methane oxidation, *Nature*, 293, 289-291,  
542 10.1038/293289a0, 1981.

543 Beck, M. and Brumsack, H.-J.: Biogeochemical cycles in sediment and water column of the Wadden Sea: The  
544 example Spiekeroog Island in a regional context, *Ocean & Coastal Management*, 68, 102-113,  
545 10.1016/j.ocecoaman.2012.05.026, 2012.

546 Boetius, A. and Wenzhöfer, F.: Seafloor oxygen consumption fuelled by methane from cold seeps, *Nature*  
547 *Geoscience*, 6, 725-734, 10.1038/ngeo1926, 2013.

548 Borges, A. V., Speeckaert, G., Champenois, W., Scranton, M. I., and Gypens, N.: Productivity and Temperature as  
549 Drivers of Seasonal and Spatial Variations of Dissolved Methane in the Southern Bight of the North Sea,  
550 *Ecosystems*, 21, 583-599, 10.1007/s10021-017-0171-7, 2018.

551 Bussmann, I.: Methane Release through Resuspension of Littoral Sediment, *Biogeochemistry*, 74, 283-302,  
552 10.1007/s10533-004-2223-2, 2005.

553 Canadell, J. G., Monteiro, P. M. S., Costa, M. H., Cotrim da Cunha, L., Cox, P. M., Eliseev, A. V., Henson, S.,  
554 Ishii, M., Jaccard, S., Koven, C., Lohila, A., Patra, P. K., Piao, S., Rogelj, J., Syampungani, S., Zaehle, S., and  
555 Zickfeld, K.: Global Carbon and other Biogeochemical Cycles and Feedbacks. In *Climate Change 2021: The*  
556 *Physical Science Basis. Contribution of Working Group I to the Sixth Assessment Report of the*  
557 *Intergovernmental Panel on Climate Change* [Masson-Delmotte, V., P. Zhai, A. Pirani, S.L. Connors, C. Péan, S.  
558 Berger, N. Caud, Y. Chen, L. Goldfarb, M.I. Gomis, M. Huang, K. Leitzell, E. Lonnoy, J.B.R. Matthews, T.K.  
559 Maycock, T. Waterfield, O. Yelekçi, R. Yu, and B. Zhou (eds.)], Cambridge University Press, pp. 673-816,  
560 doi:10.1017/9781009157896.007, 2021.

561 Crespo-Medina, M., Meile, C. D., Hunter, K. S., Diercks, A. R., Asper, V. L., Orphan, V. J., Tavormina, P. L.,  
562 Nigro, L. M., Battles, J. J., Chanton, J. P., Shiller, A. M., Joung, D. J., Amon, R. M. W., Bracco, A., Montoya, J.  
563 P., Villareal, T. A., Wood, A. M., and Joye, S. B.: The rise and fall of methanotrophy following a deepwater oil-  
564 well blowout, *Nature Geoscience*, 7, 423-427, 10.1038/ngeo2156, 2014.

565 Duran-Matute, M., Gerkema, T., de Boer, G. J., Nauw, J. J., and Gräwe, U.: Residual circulation and freshwater  
566 transport in the Dutch Wadden Sea: a numerical modelling study, *Ocean Sci.*, 10, 611-632, 10.5194/os-10-611-  
567 2014, 2014.

568 Etminan, M., Myhre, G., Highwood, E. J., and Shine, K. P.: Radiative forcing of carbon dioxide, methane, and  
569 nitrous oxide: A significant revision of the methane radiative forcing, *Geophysical Research Letters*, 43, 12,614-  
570 612,623, 10.1002/2016gl071930, 2016.

571 Gräwe, U., Flöser, G., Gerkema, T., Duran-Matute, M., Badewien, T. H., Schulz, E., and Burchard, H.: A  
572 numerical model for the entire Wadden Sea: Skill assessment and analysis of hydrodynamics, *Journal of*  
573 *Geophysical Research: Oceans*, 121, 5231-5251, 10.1002/2016jc011655, 2016.

574 Green, J. D.: Headspace analysis | Static, in: *Encyclopedia of Analytical Science (Second Edition)*, edited by:  
575 Worsfold, P., Townshend, A., and Poole, C., Elsevier, Oxford, 229-236, <https://doi.org/10.1016/B0-12-369397-7/00254-5>, 2005.

577 Gründger, F., Probandt, D., Knittel, K., Carrier, V., Kalenitchenko, D., Silyakova, A., Serov, P., Ferré, B.,  
578 Svenning, M. M., and Niemann, H.: Seasonal shifts of microbial methane oxidation in Arctic shelf waters above  
579 gas seeps, *Limnology and Oceanography*, 66, 1896-1914, 10.1002/lno.11731, 2021.

580 Grunwald, M., Dellwig, O., Liebezeit, G., Schnetger, B., Reuter, R., and Brumsack, H.-J.: A novel time-series  
581 station in the Wadden Sea (NW Germany): First results on continuous nutrient and methane measurements,  
582 *Marine Chemistry*, 107, 411-421, 10.1016/j.marchem.2007.04.003, 2007.

583 Grunwald, M., Dellwig, O., Beck, M., Dippner, J. W., Freund, J. A., Kohlmeier, C., Schnetger, B., and Brumsack,  
584 H.-J.: Methane in the southern North Sea: Sources, spatial distribution and budgets, *Estuarine, Coastal and Shelf*  
585 *Science*, 81, 445-456, 10.1016/j.ecss.2008.11.021, 2009.

586 Hanson, R. S. and Hanson, T. E.: Methanotrophic Bacteria, *Microbiological reviews*, 60, 439-471, 1996.

587 He, R., Wooller, M. J., Pohlman, J. W., Quensen, J., Tiedje, J. M., and Leigh, M. B.: Shifts in Identity and Activity  
588 of Methanotrophs in Arctic Lake Sediments in Response to Temperature Changes, *Applied and Environmental*  
589 *Microbiology*, 78, 4715-4723, doi:10.1128/AEM.00853-12, 2012.

590 Hirayama, H., Fuse, H., Abe, M., Miyazaki, M., Nakamura, T., Nunoura, T., Furushima, Y., Yamamoto, H., and  
591 Takai, K.: *Methylomarinum vadi* gen. nov., sp. nov., a methanotroph isolated from two distinct marine  
592 environments, *International Journal of Systematic and Evolutionary Microbiology*, 63, 1073-1082,  
593 <https://doi.org/10.1099/ijs.0.040568-0>, 2013.

594 Ho, A., Mo, Y., Lee, H. J., Sauheitl, L., Jia, Z., and Horn, M. A.: Effect of salt stress on aerobic methane oxidation  
595 and associated methanotrophs; a microcosm study of a natural community from a non-saline environment, *Soil*  
596 *Biology and Biochemistry*, 125, 210-214, <https://doi.org/10.1016/j.soilbio.2018.07.013>, 2018.

597 Jacques, C., Gkritzalis, T., Tison, J.-L., Hartley, T., van der Veen, C., Röckmann, T., Middelburg, J. J., Cattrijsse,  
598 A., Egger, M., Dehairs, F., and Sapart, C. J.: Carbon and Hydrogen Isotope Signatures of Dissolved Methane in  
599 the Scheldt Estuary, *Estuaries and Coasts*, 44, 137-146, 10.1007/s12237-020-00768-3, 2021.

600 Jähne, B., Münnich, K. O., Böisinger, R., Dutzi, A., Huber, W., and Libner, P.: On the parameters influencing air-  
601 water gas exchange, *Journal of Geophysical Research: Oceans*, 92, 1937-1949, 10.1029/JC092iC02p01937,  
602 1987.

603 James, R. H., Bousquet, P., Bussmann, I., Haeckel, M., Kipfer, R., Leifer, I., Niemann, H., Ostrovsky, I., Piskozub,  
604 J., Rehder, G., Treude, T., Vielstädte, L., and Greinert, J.: Effects of climate change on methane emissions from  
605 seafloor sediments in the Arctic Ocean: A review, *Limnology and Oceanography*, 61, S283-S299,  
606 10.1002/lno.10307, 2016.

607 Jordan, S. F. A., Gräwe, U., Treude, T., van der Lee, E. M., Schneider von Deimling, J., Rehder, G., and Schmale,  
608 O.: Pelagic Methane Sink Enhanced by Benthic Methanotrophs Ejected From a Gas Seep, *Geophysical Research*  
609 *Letters*, 48, e2021GL094819, 10.1029/2021GL094819, 2021.

610 Jordan, S. F. A., Treude, T., Leifer, I., Janssen, R., Werner, J., Schulz-Vogt, H., and Schmale, O.: Bubble-mediated  
611 transport of benthic microorganisms into the water column: Identification of methanotrophs and implication of  
612 seepage intensity on transport efficiency, *Scientific Reports*, 10, 4682, 10.1038/s41598-020-61446-9, 2020.

613 Knief, C.: Diversity and Habitat Preferences of Cultivated and Uncultivated Aerobic Methanotrophic Bacteria  
614 Evaluated Based on pmoA as Molecular Marker, *Frontier Microbiology*, 6, 1346, 10.3389/fmicb.2015.01346,  
615 2015.

616 Lan, X., Thoning, K. W., and Dlugokencky, E. J.: Trends in globally-averaged CH<sub>4</sub>, N<sub>2</sub>O, and SF<sub>6</sub> determined  
617 from NOAA Global Monitoring Laboratory measurements, Version 2023-06, [https://doi.org/10.15138/P8XG-  
618 AA10](https://doi.org/10.15138/P8XG-AA10), 2022.

619 Lê, S., Josse, J., and Husson, F.: FactoMineR: An R Package for Multivariate Analysis, *Journal of Statistical*  
620 *Software*, 25, 1 - 18, 10.18637/jss.v025.i01, 2008.

621 Mariotti, A., Germon, J. C., Hubert, P., Kaiser, P., Letolle, R., Tardieux, A., and Tardieux, P.: Experimental  
622 determination of nitrogen kinetic isotope fractionation: Some principles; illustration for the denitrification and  
623 nitrification processes, *Plant and Soil*, 62, 413-430, 10.1007/BF02374138, 1981.

624 Materić, D., Holzinger, R., and Niemann, H.: Nanoplastics and ultrafine microplastic in the Dutch Wadden Sea –  
625 The hidden plastics debris?, *Science of The Total Environment*, 846, 157371,  
626 <https://doi.org/10.1016/j.scitotenv.2022.157371>, 2022.

627 Mau, S., Blees, J., Helmke, E., Niemann, H., and Damm, E.: Vertical distribution of methane oxidation and  
628 methanotrophic response to elevated methane concentrations in stratified waters of the Arctic fjord Storfjorden  
629 (Svalbard, Norway), *Biogeosciences*, 10, 6267-6278, 10.5194/bg-10-6267-2013, 2013.

630 Middelburg, J. J., Nieuwenhuize, J., Iversen, N., Høgh, N., de Wilde, H., Helder, W., Seifert, R., and Christof, O.:  
631 Methane distribution in European tidal estuaries, *Biogeochemistry*, 59, 95-119, 10.1023/A:1015515130419,  
632 2002.

633 Murray, N. J., Phinn, S. R., DeWitt, M., Ferrari, R., Johnston, R., Lyons, M. B., Clinton, N., Thau, D., and Fuller,  
634 R. A.: The global distribution and trajectory of tidal flats, *Nature*, 565, 222-225, 10.1038/s41586-018-0805-8,  
635 2019.

636 Niemann, H., Steinle, L., Blees, J., Bussmann, I., Treude, T., Krause, S., Elvert, M., and Lehmann, M. F.: Toxic  
637 effects of lab-grade butyl rubber stoppers on aerobic methane oxidation, *Limnology and Oceanography*:  
638 *Methods*, 13, 40-52, 10.1002/lom3.10005, 2015.

639 Osudar, R., Klings, K. W., Wagner, D., and Bussmann, I.: Effect of salinity on microbial methane oxidation in  
640 freshwater and marine environments, *Aquatic Microbial Ecology*, 80, 181-192, 2017.

641 Osudar, R., Matoušů, A., Alawi, M., Wagner, D., and Bussmann, I.: Environmental factors affecting methane  
642 distribution and bacterial methane oxidation in the German Bight (North Sea), *Estuarine, Coastal and Shelf*  
643 *Science*, 160, 10-21, <https://doi.org/10.1016/j.ecss.2015.03.028>, 2015.

644 Philippart, C. J. M., van Iperen, J. M., Cadée, G. C., and Zuur, A. F.: Long-term Field Observations on Seasonality  
645 in Chlorophyll-a Concentrations in a Shallow Coastal Marine Ecosystem, the Wadden Sea, *Estuaries and Coasts*,  
646 33, 286-294, 10.1007/s12237-009-9236-y, 2009.

647 Reeburgh, W. S.: Oceanic Methane Biogeochemistry, *Chemical Reviews*, 107, 486-513, 10.1021/cr050362v, 2007.

648 Röckmann, T., Eyer, S., van der Veen, C., Popa, M. E., Tuzson, B., Monteil, G., Houweling, S., Harris, E.,  
649 Brunner, D., Fischer, H., Zazzeri, G., Lowry, D., Nisbet, E. G., Brand, W. A., Necki, J. M., Emmenegger, L.,  
650 and Mohn, J.: In situ observations of the isotopic composition of methane at the Cabauw tall tower site,  
651 *Atmospheric Chemistry Physics*, 16, 10469-10487, 10.5194/acp-16-10469-2016, 2016.

652 Rosentreter, J. A., Borges, A. V., Deemer, B. R., Holgerson, M. A., Liu, S., Song, C., Melack, J., Raymond, P. A.,  
653 Duarte, C. M., Allen, G. H., Olefeldt, D., Poulter, B., Battin, T. I., and Eyre, B. D.: Half of global methane

654 emissions come from highly variable aquatic ecosystem sources, *Nature Geoscience*, 14, 225-230,  
655 10.1038/s41561-021-00715-2, 2021.

656 Røy, H., Lee, J. S., Jansen, S., and de Beer, D.: Tide-driven deep pore-water flow in intertidal sand flats,  
657 *Limnology and Oceanography*, 53, 1521-1530, <https://doi.org/10.4319/lo.2008.53.4.1521>, 2008.

658 Santos, I. R., Beck, M., Brumsack, H.-J., Maher, D. T., Dittmar, T., Waska, H., and Schnetger, B.: Porewater  
659 exchange as a driver of carbon dynamics across a terrestrial-marine transect: Insights from coupled 222Rn and  
660 pCO<sub>2</sub> observations in the German Wadden Sea, *Marine Chemistry*, 171, 10-20,  
661 <https://doi.org/10.1016/j.marchem.2015.02.005>, 2015.

662 Saunois, M., Stavert, A. R., Poulter, B., Bousquet, P., Canadell, J. G., Jackson, R. B., Raymond, P. A.,  
663 Dlugokencky, E. J., Houweling, S., Patra, P. K., Ciais, P., Arora, V. K., Bastviken, D., Bergamaschi, P., Blake,  
664 D. R., Brailsford, G., Bruhwiler, L., Carlson, K. M., Carrol, M., Castaldi, S., Chandra, N., Crevoisier, C., Crill,  
665 P. M., Covey, K., Curry, C. L., Etiope, G., Frankenberg, C., Gedney, N., Hegglin, M. I., Höglund-Isaksson, L.,  
666 Hugelius, G., Ishizawa, M., Ito, A., Janssens-Maenhout, G., Jensen, K. M., Joos, F., Kleinen, T., Krummel, P. B.,  
667 Langenfelds, R. L., Laruelle, G. G., Liu, L., Machida, T., Maksyutov, S., McDonald, K. C., McNorton, J.,  
668 Miller, P. A., Melton, J. R., Morino, I., Müller, J., Murguía-Flores, F., Naik, V., Niwa, Y., Noce, S., O'Doherty,  
669 S., Parker, R. J., Peng, C., Peng, S., Peters, G. P., Prigent, C., Prinn, R., Ramonet, M., Regnier, P., Riley, W. J.,  
670 Rosentretter, J. A., Segers, A., Simpson, I. J., Shi, H., Smith, S. J., Steele, L. P., Thornton, B. F., Tian, H.,  
671 Tohjima, Y., Tubiello, F. N., Tsuruta, A., Viovy, N., Voulgarakis, A., Weber, T. S., van Weele, M., van der  
672 Werf, G. R., Weiss, R. F., Worthy, D., Wunch, D., Yin, Y., Yoshida, Y., Zhang, W., Zhang, Z., Zhao, Y., Zheng,  
673 B., Zhu, Q., Zhu, Q., and Zhuang, Q.: The Global Methane Budget 2000–2017, *Earth System Science Data*, 12,  
674 1561-1623, 10.5194/essd-12-1561-2020, 2020.

675 Schmale, O., Leifer, I., Deimling, J. S. v., Stolle, C., Krause, S., Kießlich, K., Frahm, A., and Treude, T.: Bubble  
676 Transport Mechanism: Indications for a gas bubble-mediated inoculation of benthic methanotrophs into the  
677 water column, *Continental Shelf Research*, 103, 70-78, 10.1016/j.csr.2015.04.022, 2015.

678 Steinle, L., Maltby, J., Treude, T., Kock, A., Bange, H. W., Engbersen, N., Zopfi, J., Lehmann, M. F., and  
679 Niemann, H.: Effects of low oxygen concentrations on aerobic methane oxidation in seasonally hypoxic coastal  
680 waters, *Biogeosciences*, 14, 1631-1645, 10.5194/bg-14-1631-2017, 2017.

681 Steinle, L., Schmidt, M., Bryant, L., Haeckel, M., Linke, P., Sommer, S., Zopfi, J., Lehmann, M. F., Treude, T.,  
682 and Niemann, H.: Linked sediment and water-column methanotrophy at a man-made gas blowout in the North  
683 Sea: Implications for methane budgeting in seasonally stratified shallow seas, *Limnology and Oceanography*, 61,  
684 S367-S386, 10.1002/lno.10388, 2016.

685 Steinle, L., Graves, A. C., Treude, T., Ferré, B., Biastoch, A., Bussmann, I., Berndt, C., Krastel, S., James, R. H.,  
686 Behrens, E., Böning, C. W., Greinert, J., Sapart, C., Scheinert, M., Sommer, S., Lehmann, M. F., and Niemann,  
687 H.: Water column methanotrophy controlled by a rapid oceanographic switch, *Nature Geoscience*, 8, 378-382,  
688 10.1038/ngeo2420, 2015.

689 Tavormina, P. L., Hatzenpichler, R., McGlynn, S., Chadwick, G., Dawson, K. S., Connon, S. A., and Orphan, V.  
690 J.: *Methyloprofundus sedimenti* gen. nov., sp. nov., an obligate methanotroph from ocean sediment belonging to  
691 the 'deep sea-1' clade of marine methanotrophs, *International Journal of Systematic and Evolutionary*  
692 *Microbiology*, 65, 251-259, <https://doi.org/10.1099/ijs.0.062927-0>, 2015.

693 Thornton, B. F., Geibel, M. C., Crill, P. M., Humborg, C., and Mörth, C.-M.: Methane fluxes from the sea to the  
694 atmosphere across the Siberian shelf seas, *Geophysical Research Letters*, 43, 5869-5877,  
695 <https://doi.org/10.1002/2016GL068977>, 2016.

696 van Aken, H. M.: Variability of the salinity in the western Wadden Sea on tidal to centennial time scales, *Journal*  
697 *of Sea Research*, 59, 121-132, <https://doi.org/10.1016/j.seares.2007.11.001>, 2008.

698 Wanninkhof, R.: Relationship between wind speed and gas exchange over the ocean revisited, *Limnology and*  
699 *Oceanography: Methods*, 12, 351-362, 10.4319/lom.2014.12.351, 2014.

700 Weber, T., Wiseman, N. A., and Kock, A.: Global ocean methane emissions dominated by shallow coastal waters,  
701 *Nature communications*, 10, 1-10, 2019.

702 Whiticar, M. J.: Carbon and hydrogen isotope systematics of bacterial formation and oxidation of methane,  
703 *Chemical Geology*, 161, 291-314, 10.1016/S0009-2541(99)00092-3, 1999.

704 Wiesenberg, D. A. and Guinasso, N. L.: Equilibrium Solubilities of Methane, Carbon Monoxide, and Hydrogen in  
705 Water and Sea Water, *Journal of Chemical & Engineering Data*, 24, 356-360, 1979.

706 Wu, C. S., Røy, H., and de Beer, D.: Methanogenesis in sediments of an intertidal sand flat in the Wadden Sea,  
707 *Estuarine, Coastal and Shelf Science*, 164, 39-45, 10.1016/j.ecss.2015.06.031, 2015.

708 Yvon-Durocher, G., Allen, A. P., Bastviken, D., Conrad, R., Gudas, C., St-Pierre, A., Thanh-Duc, N., and del  
709 Giorgio, P. A.: Methane fluxes show consistent temperature dependence across microbial to ecosystem scales,  
710 *Nature*, 507, 488-491, 10.1038/nature13164, 2014.

711 Zhang, S., Yan, L., Cao, J., Wang, K., Luo, Y., Hu, H., Wang, L., Yu, R., Pan, B., Yu, K., Zhao, J., and Bao, Z.:  
712 Salinity significantly affects methane oxidation and methanotrophic community in Inner Mongolia lake  
713 sediments, *Frontiers in Microbiology*, 13, 10.3389/fmicb.2022.1067017, 2023.

